Global Journal of Engineering and Technology Advances
eISSN: 2582-5003
Cross Ref DOI: 10.30574/gjeta
Journal homepage: https://gjeta.com/

(RESEARCH ARTICLE)

Check for updates

Numerical modeling of steel fiber reinforced concrete spallation exposed to medium loading rate

Ammar Babiker [1,*], Aamir Dean [1,2], Ebtihag Abu-Elgasim [1] and Taghried Abdel-Magid [1,3]

[1] *College of Engineering, School of Civil Engineering, Sudan University of Science and Technology, Khartoum, Sudan.*
[2] *Elasticity and Strength of Materials Group, School of Engineering, University of Seville, Seville, Spain.*
[3] *BRE Center for Innovative Construction Materials, Department of Architecture and Civil Engineering, Faculty of Engineering, University of Bath, Bath, UK.*

Global Journal of Engineering and Technology Advances, 2022, 12(02), 001–014

Publication history: Received on 25 June 2022; revised on 29 July 2022; accepted on 31 July 2022

Article DOI: https://doi.org/10.30574/gjeta.2022.12.2.0130

Abstract

Properties of unreinforced concrete and cement-based matrix are well understood. One of the issues with the cement-based matrix is its inherently brittle failure when exposed to loading. As such, steel fibers were proposed to enhance the ductility of cement-based and concrete materials. Ever since, Fiber-Reinforced Concrete (FRC) has become a commonly used building material in many construction activities such as bridges, airport pavements, shotcrete, and many others. According to previous research, the addition of steel fibers, typically from 20 to 50 kg/m^3 into the conventional concrete, can significantly enhance many of the desired engineering properties of hardened concrete such as flexural strength, tensile strength, micro-cracks as well as splitting. This research presents a study aimed to numerically investigate the influence of steel fibers on the dynamic behavior of Plain Concrete (PC) exposed the tensile loading at medium strain-rate. The influence of steel fibers is investigated using different fiber volume fractions ranging from 0.0 to 4.5%. The Modified Split-Hopkinson-Bar (MSHB) apparatus is employed to investigate the dynamic tensile behavior of PC and Steel Fiber-Reinforced Concrete (SFRC). Validation of the finite element model and constitutive material behavior is carried out with the comparison of computed and measured experimental pull-back velocities of the specimen's free end. The results showed that impact properties of steel fibers exhibit significant improvement in the toughness and the dynamic tensile strength of concrete and higher fiber volume fraction is more effective in enhancing the mechanical properties of SFRC composite.

Keywords: Fiber-reinforced Concrete; Steel fibers; Strain-rate; Spallation; Pull-back velocity; Split-Hopkinson-Bar

1. Introduction

The split Hopkinson bar (SHB) is widely used for experimental characterization of the mechanical behavior of engineering materials exposed to high and medium loading rates. It is also known as the Kolsky apparatus since Kolsky (1) was introduced in 1949. The SHB apparatus is modified by omitting it is transmitter bar to perform a concrete spalling test using the so-called Modified Split-Hopkinson-Bar (MSHB). The MSHB is a direct test to investigate the dynamic tensile behavior of concrete and fiber-reinforced concrete (FRC) materials. The MSHB spall configuration includes a striker bar, incident bar, and a slender specimen, see Figure 1. A compressive stress wave produced by a striker hitting the incident bar propagates along the bar. When it reaches the specimen, a part of it is transmitted into the specimen, while, the rest is reflected into the incident bar as tensile waves owing to impedance difference. When the transmitted compressive stress wave arrives at the free end of the specimen, it is reflected as tensile stress, which causes fracture of the specimen if the maximum tensile stress is equal to the dynamic tensile strength of the material.

* Corresponding author: Ammar Babiker
School of Civil Engineering, College of Engineering, Sudan University of Science and Technology, Khartoum, Sudan.

Figure 1 illustrates the propagation of the stress waves during the spall test. Several experimental and numerical spallation investigations have been conducted (2–10). Most of these studies used cementitious materials such as mortar and concrete. However, very limited research has been carried out using FRC composites, see (11,12). It has been reported by many researchers that the addition of fibers into the brittle matrix can significantly increase the tensile strength, ductility, toughness, and post-cracking behavior (13,14).

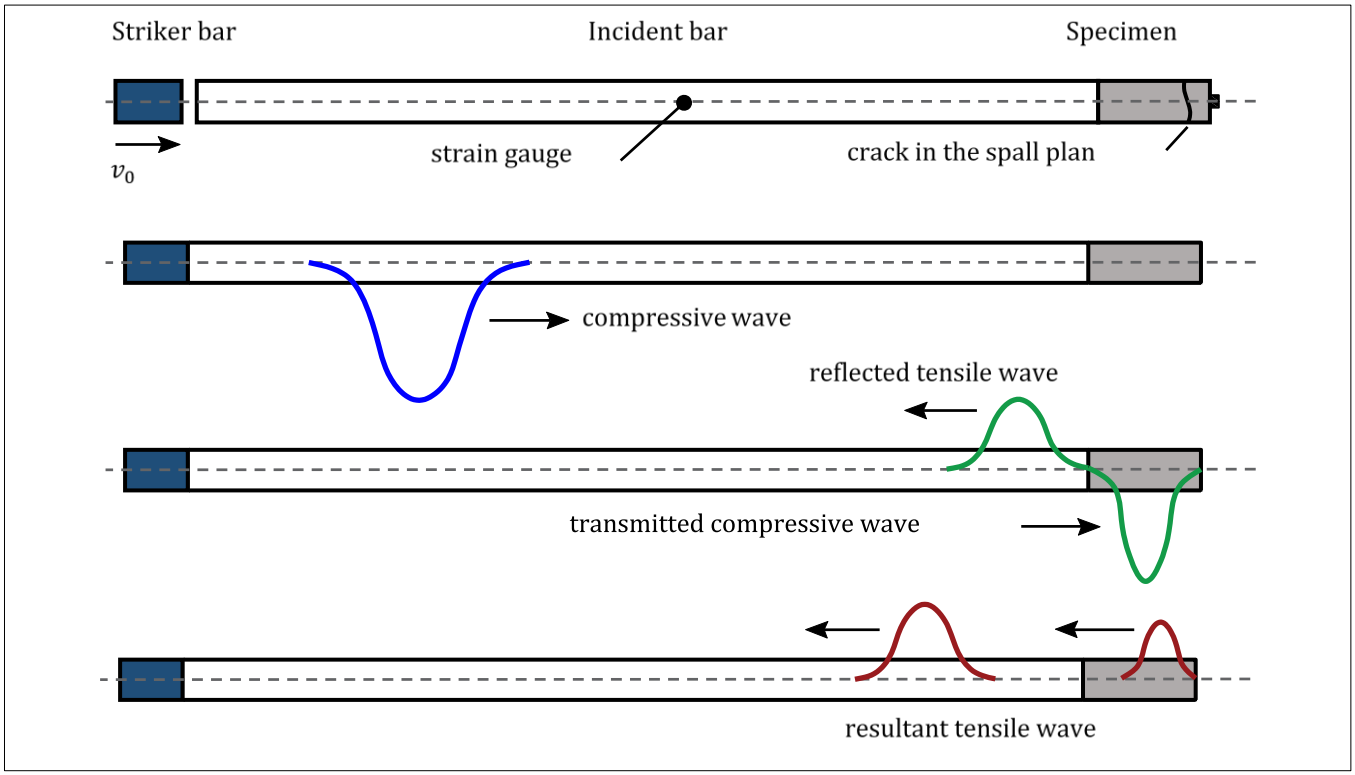

Figure 1 Wave propagation in spallation experiment

This work emphasizes the numerical investigation of Steel Fiber-Reinforced Concrete (SFRC) composites subjected to dynamic tensile loading using the MSHB. To study the influence of adding short steel fiber on the conventional concrete matrix, different dosages of steel fibers have been investigated. The finite element simulations were performed with a similar setup as that presented in our previous research (15).

2. Dynamic tensile strength

2.1. Indirect method

The dynamic tensile strength can be evaluated using different methods. A linear acoustic approximation was given in Eq. (1) introduced by Novikov et al. (16) to calculate the dynamic tensile strength in the spallation test using the pull-back velocity recorded on the rear face of the specimen. It has been applied by many researchers, for instance, Schuler et al. (2), and Babiker et al. (15).

$$\sigma_{dyn} = \frac{1}{2}\rho C \Delta v_{pb} \qquad (1)$$

where ρ is the specimen density, C is the wave velocity, and Δv_{pb} is the pull-back velocity, is the difference between the maximum and the rebound velocities.

2.2. Direct method

The direct method deduces the dynamic tensile strength directly from stress-time wave history at various locations along the specimen. Such a method is shown in Figure 2.

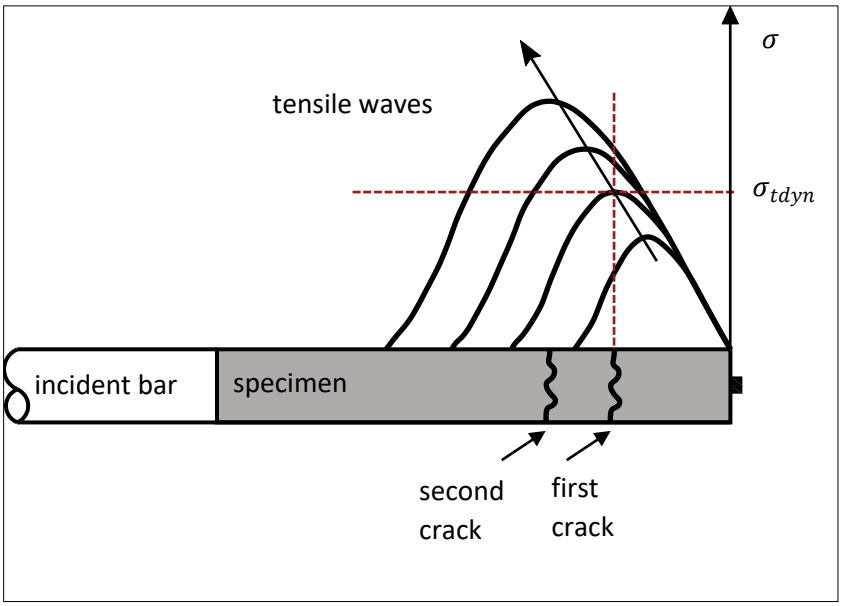

Figure 2 Dynamic tensile strength calculation

3. Wave velocity and dynamic Young's modulus

3.1. Wave velocity

The elastic wave velocity of the specimen C can be calculated from the time-history signals recorded at the beginning of the specimen and the particle velocity at the free surface end of the specimen using Eq. (2).

$$C = \frac{L}{\Delta t} \qquad (2)$$

where L is the specimen length and Δt is the time that the wave needs to propagate from the beginning to the end of the specimen. For more details, see Babiker et al. (15).

3.2. Dynamic Young's modulus

The dynamic Young's modulus is given by Eq. (3).

$$E_{dyn} = \rho C^2 \qquad (3)$$

4. Numerical simulation of spallation

This section presents the numerical simulation procedure of the wave propagation in the MSHB apparatus. The analysis was performed using the Ls-Dyna explicit solver suitable to solve dynamic problems that involve wave propagation. The simulation of spallation is performed with a similar setup as given in Babiker et al. (15), in which numerical study on spallation test of plain concrete is presented. The modeling aspects, including the finite element discretization, elements type, boundary conditions, material formulations, and contact algorithms are briefly discussed in the following.

4.1. Model geometry

The 3D MSHB model was developed using the Ls-PrePost processor. The apparatus of the spallation test includes a striker bar, incident bar, and a slender rod specimen as shown in Figure 1. Detailed dimensions of the bars and specimen are provided in Table 1.

Table 1 Dimensions of MSHB model.

Component	Length [mm]	Diameter [mm]
Striker bar	60	75
Incident bar	5500	75
Specimen	250	75

4.2. Fiber geometry generation

The steel fibers are modeled as beam elements. Each fiber is assumed to be a straight and round element of a uniform cross-sectional area. With the fiber dimension and the percentage of fiber volume fraction in the SFRC specimen, the total number of fibers can be determined. Based on the concepts of the random number, the number of random numbers is equal to the number of fibers calculated according to desired fiber percentage. Each of the fibers having a fixed length can be oriented randomly within the SFRC specimen domain.

It is well known that fibers are highly dispersive in concrete matrix; therefore, a MATLAB program is developed to generate the random position and orientation of each fiber. The tacking and placing process of fibers can be summarized as follows:

- Step 1. Calculate the quantity of the fibers according to the fiber dosage or fiber volume fraction.
- Step 2. Generate the random positions and orientations for all the fibers within the SFRC specimen domain.
- Step 3. Place all the fibers one by one into the SFRC specimen and check to ensure the fiber is located within the specimen boundary.
- Step 4. Repeat steps 2 and 3 until the volume of the generated fibers is equal to the specified fiber dosage.
- Step 5. Output the data of random positions and orientations of all generated fibers.

As a termination process, the random generator fulfills two conditions, they are: (1) the generation of fibers is terminated when the advanced specified dosage of fiber is reached, and (2) the crossing between fibers is not allowed, i.e., if two fibers are crossing, one of them is removed and re-generate. Finally, the generated fibers are exported to Ls-Dyna to define their section and material properties. Figure 3 shows an example of generated SFRC specimens with different fiber contents.

4.3. Elements and mesh

The striker and incident bars were all modeled using single integration eight-node hexahedral solid elements with the element formulation type ELFORM=1 in Ls-Dyna code.

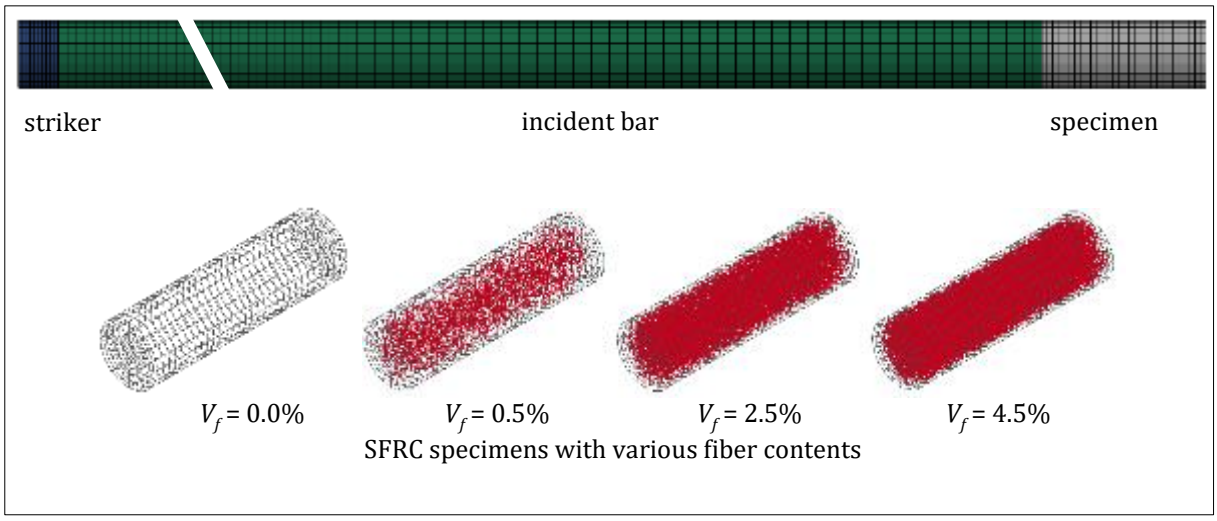

Figure 3 Finite element discretization of the spallation setup

SFRC specimens were constructed using straight and round steel fibers distributed randomly with the specimen domain. Each fiber has a length of 16 mm and a diameter of 0.5 mm with an aspect ratio of 32. Three different fiber volume fractions were investigated, namely 0.5%, 2.5%, and 4.5% in addition to the reference model, i.e., the model with 0.0% of fibers. The steel fibers were realized using a two-node beam element with Hughes-Liu formulation. The mesh size chosen for the concrete portion was about 6 mm.
An overview of the number of elements for any part of each MSHB model is given in Table 2. The reference discretization along with SFRC specimens is shown in Figure 3.

Table 2 Number of elements used in each model

Component	Fiber volume fraction V_f [%]			
	0.0	**0.5**	**2.5**	**4.5**
Striker bar	3150	3150	3150	3150
Incident bar	1050	1050	1050	1050
Concrete	42000	42000	42000	42000
Steel fibers	0.000	1758	8789	15820

The striker velocity was set to 4.1 m/s. The velocity was assigned to the striker bar nodes using Ls-Dyna keyword *INITIAL_VELOCITY_GENERATION. It should be noted that an initial gap of 1 mm is given at the interface between the striker and incident bars.

5. Contact algorithms

In SFRC modeling, the bond between the steel fibers and the surrounding concrete matrix is crucial and has a significant impact on the overall structural behavior. Ls-Dyna finite element code offers different methods for including steel fibers into a concrete matrix. Herein work, the beam elements representing the steel fibers were perfectly bonded to the surrounding solid Lagrangian elements that represent concrete matrix using the constraint method. This operation was conducted with the help of the *CONSTRAINED_BEAM_IN_SOLID keyword available in Ls-Dyna explicit code. The interface between the striker and incident bars was modeled using the standard contact algorithm *SINGLE_SURFACE, whereas the SFRC specimen has its interfacing nodes in common with the incident bar to guarantee a perfect glue.

6. Constitutive material model

A material model, also known as a constitutive model, is the description of the physical of a material. In this research, three different material formulations are adopted to define the mechanical properties for each part of the 3D finite element model. The following describes the material model used in each part of the finite element model.

6.1. Material model for concrete

For the current study, the constitutive model for concrete is the most crucial. Nowadays, a wide range of material models that can be used for concrete is available in Ls-Dyna finite element code. In this research, the Continuous Surface Cap Model (CSCM), i.e., *MAT_145 was selected to define the mechanical properties of concrete material. The CSCM material model, developed originally by Schwer and Murray (17–19), is widely known as Schwer & Murray Cap Model. It is a three-invariant extension of the Geologic Cap Model (*MAT_025). This formulation includes viscoelasticity to model the strain-rate effect and also employs damage mechanics to model strain softening and modulus degradation in both tension and compression regimes (20,21). In the CSCM material model, an elliptical cap surface is used to account for the plastic volume change which is related to pore collapse in concrete materials. The CSCM also has capability to model different geomaterials, including soils and rock (20).
The material formulation is provided with a combined yield surface; they are, the failure surface of the smooth cap hardening $F_f(J_1)$ and the isotropic hardening or cap surface $F_c(J_1, \kappa)$ as can be seen in **Error! Reference source not found.**.
The failure surface of the smooth cap model is defined in terms of the first invariant J_1 as an exponential function.

$$F_f(J_1) = \sqrt{J_2} = \alpha - \gamma \exp(-\beta J_1) + \theta J_1 \quad (4)$$

with

$$J_1 = \sigma_{ii} = 3P$$

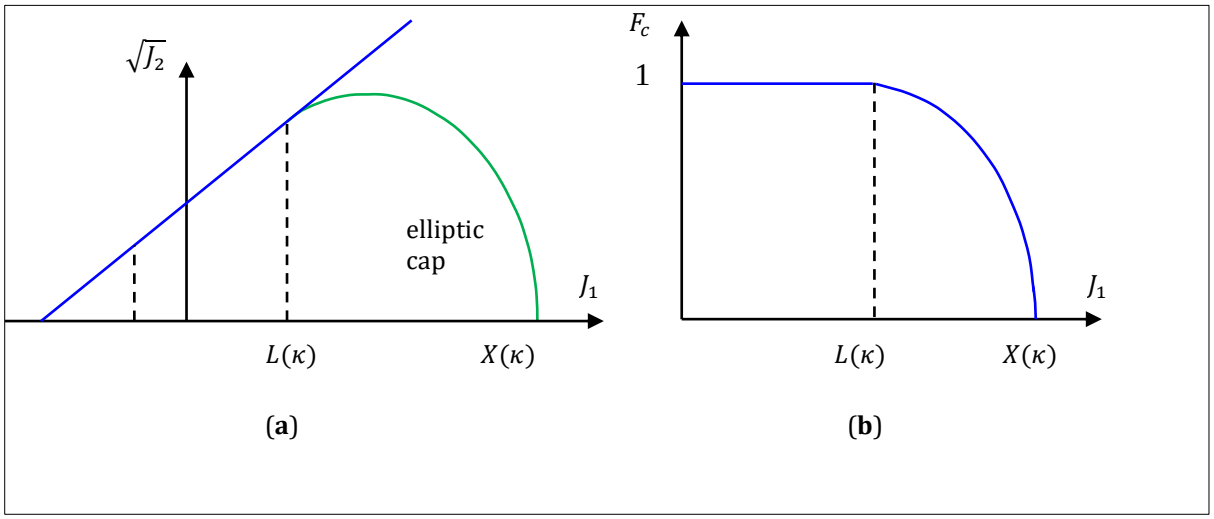

Figure 4 Continuous surface cap model, adapted from Schwer and Murray (17); (a) single surface smooth cap failure function and (b) non-dimensional function of the smooth cap failure function

The cap surface, i.e., the isotropic hardening of the model depends on a non-dimensional function, as shown in **Error! Reference source not found.**(b), and is a two-part function that is either unity or ellipse. The cap surface is mathematically described as:

$$F_c(J_1, \kappa) = \begin{cases} 1, & J_1 \le L(\kappa) \\ 1 - \dfrac{[J_1 - L(\kappa)]^2}{[X(\kappa - L(\kappa)]^2}, & J_1 > L(\kappa) \end{cases} \quad (5)$$

where κ denotes the hardening parameter that controls the motion of the cap surface, $L(\kappa)$ and $X(\kappa)$ defines the geometry of the cap surface. The function F_c is unity for J_1 less than or equal $L(\kappa)$ and elliptical between the range $L(\kappa) \le J_1 \le X(\kappa)$. Another parameter (material constant) S needs to be considered to define the ellipticity of the cap surface, which is related to the geometry parameters $L(\kappa)$ and $X(\kappa)$ as:

$$X(\kappa) = L(\kappa) + SF_f\big(L(\kappa)\big) \quad (6)$$

with

$$L(\kappa) = \begin{cases} \kappa, & \kappa > \kappa_0 \\ \kappa_0, & \text{Otherwise} \end{cases} \quad (7)$$

in which κ_0 is the value of J_1 at the beginning of the interaction between the failure and cap surfaces. The evolution of the cap motion is defined by the isotropic hardening rule as follows, while without cap motion the pressure-volumetric strain curve is perfect plastic:

$$\varepsilon_v^p = W(1 - \exp(1 - D_1[X - X_0] - D_2[X - X_0]^2)) \quad (8)$$

where $\varepsilon_p^p = tr\ \varepsilon_{ij}^p$ is the plastic volumetric strain, W is the maximum plastic volumetric strain, X_0 is the initial abscissa intercept of the cap surface, D_1 and D_2 are shape factors.

Strain softening and modulus reduction of concrete is modeled with an isotropic damage formulation in the model. Strain softening corresponds to a post-peal decrease in strength and modulus reduction denotes a reduction of elastic modulus in cyclic loading conditions.

The damage criterion is based on the damage energy release rate-based approach introduced by Simo and Ju (22). The smooth cap model shown in **Error! Reference source not found.**(a) is a result of combining the failure and hardening surfaces to form a continuous derivative function given by:

$$f(J_1, J_2, \kappa) = J_2 - F_f^2 F_c R^2 \qquad (9)$$

with

$$J_2 = \frac{1}{2} S_{ij} S_{ij}$$

Where R is the Rubin scaling function, see, (23) J_2 is the second invariant of the deviatoric stress tensor. The deviatoric stress tensor S_{ij} can be related to the stress σ_{ij} tensor as follows:

$$S_{ij} = \sigma_{ij} - P\delta_{ij}$$

Table 3 Material Parameters used for concrete

Parameter	**Value**
Unit weight, ρ [Kg/m^3]	2273
Modulus of elasticity, E [GPa]	36
Poisson's ratio, υ	0.2
Tensile strength, f_t [MPa]	3.5
Compressive strength, f_c [MPa]	50
Shear failure Parameter, α [GPa]	0.011092
Shear failure Parameter, θ	0.333873
Shear failure Parameter, γ [GPa]	0.0052711
Shear failure Parameter, β [GPa^{-1}]	32.354
Torsion scaling parameter, α_1	8.2e-4
Torsion scaling parameter, θ_1 [GPa^{-1}]	0.0
Torsion scaling parameter, γ_1	2.41e-4
Torsion scaling parameter, β_1 [GPa^{-1}]	9.94933
Tri-axial extension scaling parameter, α_2	7.6e-4
Tri-axial extension scaling parameter, θ_2 [GPa^{-1}]	0.0
Tri-axial extension scaling parameter, γ_2	2.6e-4
Tri-axial extension scaling parameter, β_2 [GPa^{-1}]	8.6179304
Initial cap surface, X_0 [GPa]	0.092767
Plastic volume strain parameter, D_1 [GPa^{-1}]	0.611
Plastic volume strain parameter, D_2 [GPa^{-1}]	2.23

Plastic volume strain parameter, w [GPa^{-2}]	0.065
Initial cap surface ellipticity, R_0	2.0919199

Table 3 gives the estimated material parameters for concrete according to the experimental data obtained in (2).

6.2. Material model for steel fibers

The Piecewise Linear Plasticity Model (*MAT_024) in Ls-Dyna similarly treats the plasticity as the Elastic-Plastic Hydrodynamic Material Model (*MAT_010), see (20,24). The deviatoric stresses fulfill the yield function. The model can be simplified as a bilinear elastic-plastic stress-strain relationship for most of the metallic materials, as indicated in Figure 4.

$$\emptyset = \frac{1}{2} S_{ij} S_{ij} - \frac{\sigma_y^2}{3} \leq 0 \qquad (10)$$

where S_{ij} is the deviatoric stress and can be linked to the stress tensor $S_{ij} = \delta_{ij} - \sigma_{ii}/3$. The yield strength is given by Eq. (11).

$$\sigma_y = \beta\left[\sigma_0 + f_h\left(\varepsilon_{eff}^p\right)\right] \qquad (11)$$

in which β denotes the hardening parameter accounting for the strain-rate effect, σ_0 is the yield stress. The hardening function is given by Eq. (12).

$$f_h\left(\varepsilon_{eff}^p\right) = E_p\left(\varepsilon_{eff}^p\right) \qquad (12)$$

where E_p and ε_{eff}^p are the plastic hardening modulus and effective plastic strain, respectively. They are given in the following expressions:

$$E_p = \frac{E_t\, E}{E - E_t} \qquad (13)$$

$$\varepsilon_{eff}^p = \int_0^t \left(\frac{2}{3}\dot{\varepsilon}_{ij}^p\, \dot{\varepsilon}_{ij}^p\right)^{\frac{1}{2}} \qquad (14)$$

In which E is the initial elastic modulus, E_t is the tangent modulus, and $\dot{\varepsilon}_{ij}^p$ is the plastic strain-rate, which is the difference between the total and elastic strain-rate.

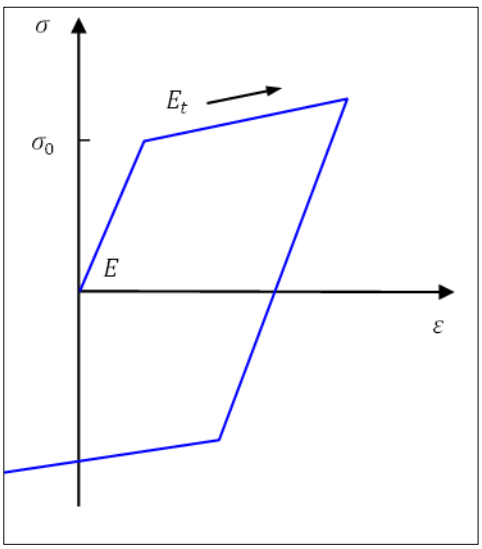

Figure 4 Uniaxial bilinear elastic-plastic stress strain, adapted from Teng et al. (24)

If needed, strain-rate effect can be accounted using Cowper and Symonds model (20) in which the yield stress is scaled as:

$$\beta = 1 + \left(\frac{\dot{\varepsilon}}{C}\right)^{1/p} \quad (15)$$

where $\dot{\varepsilon}$ is the strain rate, C and p are constants of the Cowper and Symonds model. The material parameters used for the steel fibers are listed in Table 4.

Table 4 Material parameters used for steel fibers

Parameter	Unit	Value
Unit weight	Kg/m^3	7850
Tensile strength	GPa	2.99
Modulus of elasticity	GPa	200
Yield stress	GPa	1.3
Poisson's ratio	-	0.3

6.3. Material model for striker and incident bars

The aluminum incident bar and the steel striker bar, are assumed to behave as linear elastic materials for the analysis. Their mechanical parameters were assigned using *MAT_001 in the Ls-Dyna finite element explicit code. The mechanical parameters used for the incident and striker bars are listed in Table 5 and Table 6 respectively.

Table 5 Material parameters used for incident bar

Parameter	Unit	Value
Unit weight	Kg/m^3	2720
Modulus of elasticity	GPa	72.70
Poisson's ratio	-	0.34
Elastic wave speed	m/s	5170

Table 6 Material parameters used for striker bar

Parameter	Unit	Value
Unit weight	Kg/m^3	7850
Modulus of elasticity	GPa	210
Poisson's ratio	-	0.3

7. Results and discussion

7.1. Pull-back velocity

As the wave signal propagates into the specimen, it is particle velocities arise and slow down afterward. The difference in the velocity between the maximum and the rebound velocity also known as pull-back velocity Δv_{pb} is crucial. The

pull-back velocity is the most important parameter used to deduce the dynamic tensile strength of the specimens, see Eq. (1) and Figure 5.
Figure 5 shows the pull-back velocities of the SFRC specimens obtained under varying fiber content by volume fraction. As can be seen from Figure 5 and
, the variation between the simulated pull-back velocities for various SFRC specimens is very minor and the steel fibers did not lead to significant change. This could be related to many factors such as fibers shape, fiber tensile strength, and fiber aspect ratio. Another factor would be the rate effect since fibers are rate-dependent materials.

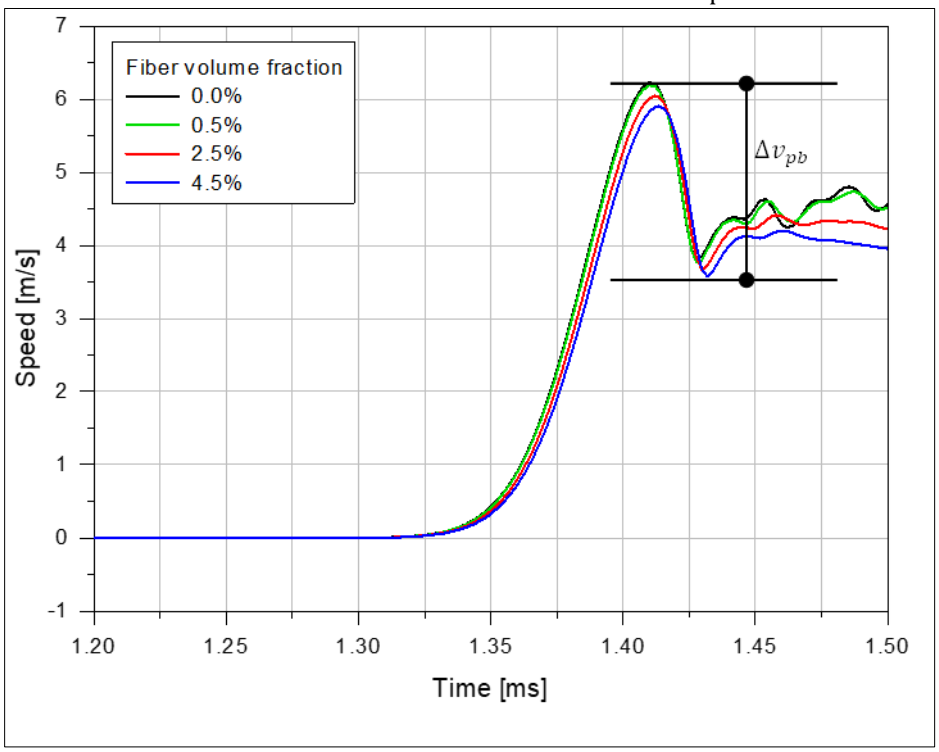

Figure 5 Recorded pull-back velocity

7.2. Dynamic tensile strength

As disused in Section **2.2,** the stress history is used to understand the specimen's behavior and to deduce the dynamic tensile strength at the fracture location.

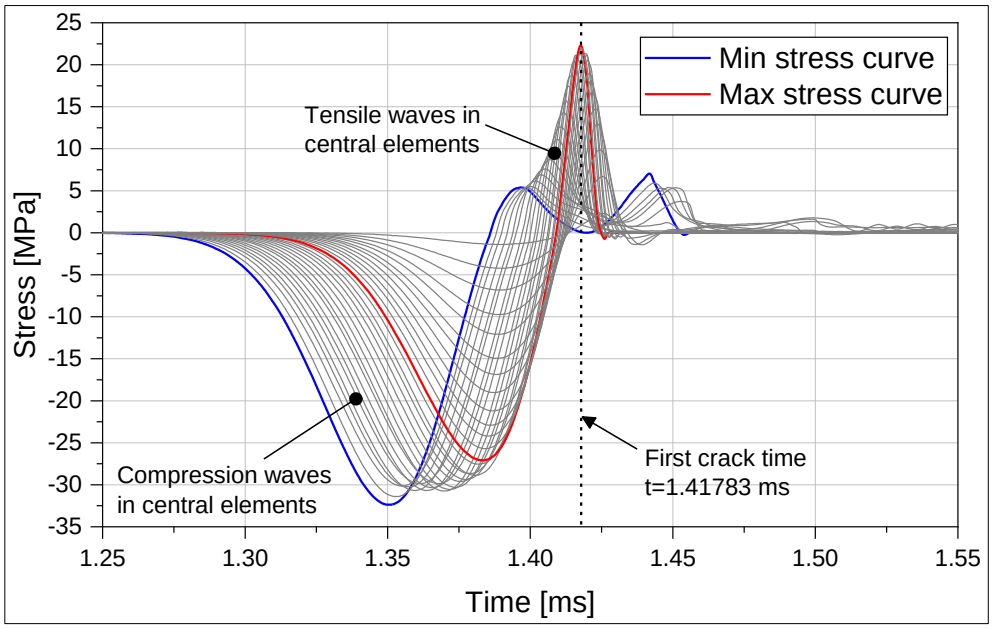

Figure 6 Longitudinal stress-time history in SFRC specimen with V_f= 4.5%.

Figure 6 shows an example of computed stress waves. The red curve indicated the stress-time evolution for the first element carrying the maximum compressive stress wave with underlying greyed average curves, whereas the red curve describes the stress-times history at the fracture location. The red curve indicates the last element, i.e., the element at the free end of the specimen at which the pull-back velocity is computed. The time at which the first fracture t_{cr} occurred is indicated by dashed lines.

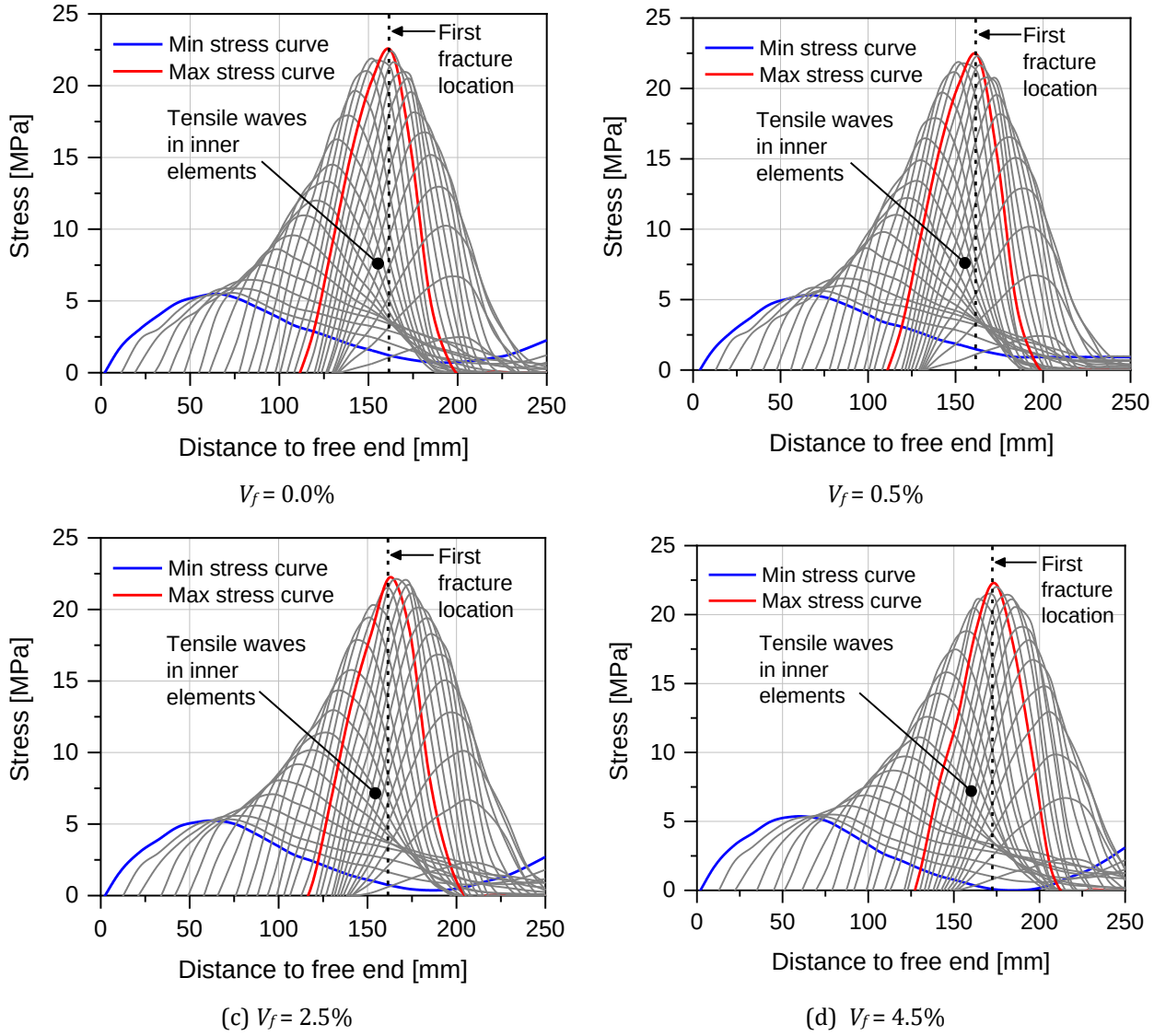

V_f = 0.0%

V_f = 0.5%

(c) V_f = 2.5%

(d) V_f = 4.5%

Figure 7 Evolution of the tensile strength for varied fiber contents.

Furthermore, Figure 7 illustrates the stress distribution along the specimen. Position 0 mm indicates the first element at the beginning of the specimen while position 250 mm corresponds to the last element at the free end of the specimen. The stress histories shown in Figure 7 were computed at the central elements (inner elements). The maximum computed dynamic tensile strengths for SFRC specimens with various fiber dosages are compared in
. By comparing the strength enhancement of the specimen without fibers with SFRC specimens, it can be concluded that there is some improvement. However, it is less than expected. Again, this can be related to many factors such as fiber geometry, fiber mechanical properties, and applied strain-rate. For further comparison, Figure 8 gives the highest longitudinal stress waves in the specimen. The values were recorded at two different times namely at 1.41568 ms and

1.41783 ms. these curves demonstrate the tensile strength enhancement that comes from the addition of steel fibers, especially after the first crack occurs.
According to the computed results, see Table 7, the dynamic tensile strengths calculated using the indirect method using Novikov's equation are in a considerable difference compared to those calculated using the stress-time history or the so-called direct method. Therefore, the assumptions of Novikov et al. (16) regarding material linearity and uniaxial stress states become more and more questionable.

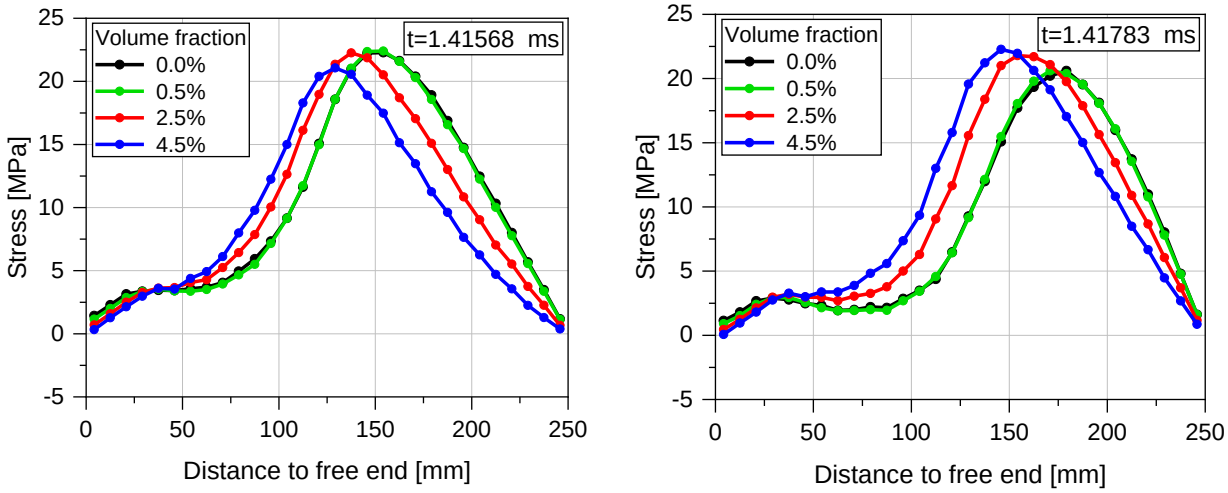

Highest element stress at 1.41568 ms

Highest element stress at 1.41783 ms

Figure 8 Influence of fiber content on the tensile strength growth.

7.3. Failure pattern

In order to further investigate the failure of the SFRC specimen, Figure 9 shows the distribution of the axial force on the steel fibers. To have a better understanding of the distribution of the axial force, the distribution is given at different intervals. As can be noticed the simulation results successfully predict the fracture locations.

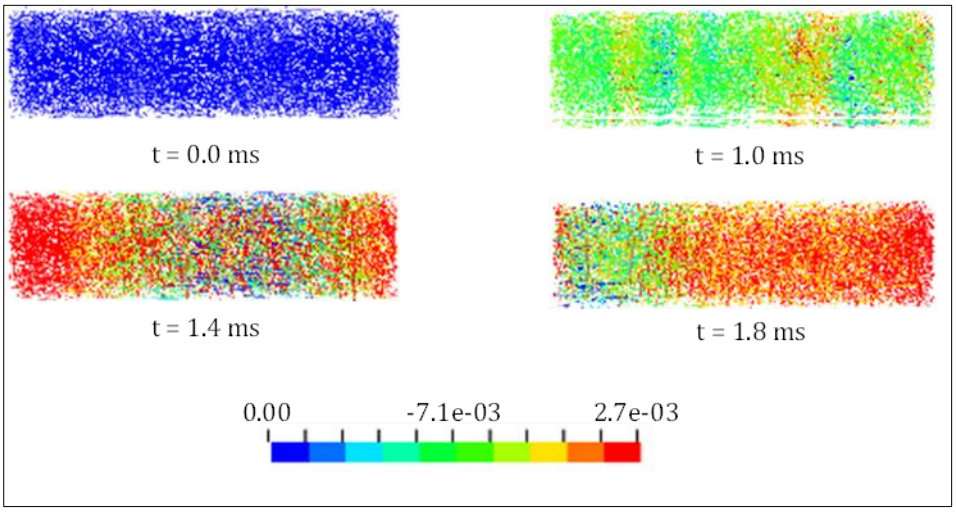

Figure 9 Distribution of the axial force on the steel fibers, V_f = 2.5%

Table 7 Computed results

Component	Fiber volume fraction V_f [%]			
	0.0	**0.5**	**2.5**	**4.5**
Pull-back velocity [m/s]	2.42	2.43	2.38	2.35
Tensile strength [MPa], using Eq. (1)	12.5	12.66	14.65	17.01
Tensile strength [MPa], using stress-time history	20.60	20.61	21.78	22.28

8. Conclusion

This research presented in this paper attempted to investigate the behavior of a mesoscopic numerical model of plain and steel fiber reinforced concrete composites at medium strain rates in spalling tests. Two different evaluation methods to calculate the dynamic tensile strength have been discussed. The impact of the steel fibers addition into the conventional concrete was investigated by using different fiber contents ranging between 0.0% to 4.5%. According to the findings of this study, the following remarks may be drawn

The obtained results demonstrated that the linear acoustic approximation introduced by Novikov et al. valid when applied to the spall experiments, whereas the estimation of the dynamic tensile strength based on the pull-back velocity may lead to underestimation of the dynamic strength compared with the direct method using the stress-time history evolution.

Although the increase is not significant, it was found that steel fibers in concrete could enhance the dynamic tensile strength of SFRC composites.

Because fiber-reinforced composites are rate dependents materials, the loading rate would have a significant influence on the evolution of the dynamic tensile strength. Thus it is suggested to use larger loading rates for proper understanding of the global behavior of SFRC specimens in spallation tests.

It is found that the employed material for concrete (*MAT_145) can well capture the behavior of plain concrete and SFRC materials exposed to tensile dynamic loading and therefore recommended for further investigation.

Finally, some aspects require more research. The influence of fiber geometry such as hooked-end steel fibers, the influence of fibers aspect ratio, and the effect of loading rate.

Compliance with ethical standards

Acknowledgments

This research was funded by the Ministry of Higher Education and Scientific Research, Sudan.

Disclosure of conflict of interest

The main author was funded by the Ministry of Higher Education, Sudan, to undertake the research resulted in this work. The authors certify that they have no conflict of interest in the subject matter or materials discussed in this manuscript.

References

[1] H Kolsky. An Investigation of the Mechanical Properties of Materials at very High Rates of Loading, *Proc. Phys. Soc. Sect. B*. 1949; 676–700.

[2] H Schuler, C Mayrhofer, K Thoma. Spall experiments for the measurement of the tensile strength and fracture energy of concrete at high strain rates, *Int. J. Impact Eng.* 2006; 32(10): 1635–1650.

[3] A. Brara, F Camborde, JR Klepaczko, C Mariotti. Experimental and numerical study of concrete at high strain rates in tension, *Mech. Mater.* 2001; 33(1): 33–45.

[4] A Brara, JR Klepaczko. Experimental characterization of concrete in dynamic tension, *Mech. Mater.* 2006; 38(3): 253–267.

[5] JR Klepaczko A Brara. Experimental method for dynamic tensile testing of concrete by spalling, *Int. J. Impact Eng.* 2001 ; 25(4): 387–409.

[6] J Weerheijm, JCAM. Van Doormaal, Tensile failure of concrete at high loading rates: New test data on strength and fracture energy from instrumented spalling tests, *Int. J. Impact Eng.* 2007; 34(3): 609–626.

[7] H Wu, Q Zhang, F Huang, Q Jin, Experimental and numerical investigation on the dynamic tensile strength of concrete, *Int. J. Impact Eng.* 2005; 32(1–4): 605–617.

[8] B Erzar, P Forquin. An experimental method to determine the tensile strength of concrete at high rates of strain, *Proc. Soc. Exp. Mech. Inc.* 2010; 67): 941–955.

[9] F Gálvez Díaz-Rubio, J Rodríguez Pérez, V Sánchez Gálvez. The spalling of long bars as a reliable method of measuring the dynamic tensile strength of ceramics, *Int. J. Impact Eng.* Feb 2002; 27(2): 161–177.

[10] L Zhang, SS Hu, DX Chen, ZQ Yu, F Liu. An experimental technique for spalling of concrete, *Exp. Mech.* 2009; 49(4): 523–532.

[11] Z Wang, N Zhou, J Wang. Using Hopkinson pressure bar to perform dynamic tensile tests on SFRC at medium strain rates, *Mag. Concr. Res.* 2012; 64(8): 657–664.

[12] I Curosu, V Mechtcherine, O Millon. Effect of fiber properties and matrix composition on the tensile behavior of strain-hardening cement-based composites (SHCCs) subject to impact loading, *Cem. Concr. Res.* 2016; 82): 23–35.

[13] Q Fang, J Zhang. Three-dimensional modelling of steel fiber reinforced concrete material under intense dynamic loading, *Constr. Build. Mater.* 2013; 44: 118–132.

[14] LF Friedrich C Wang. Continuous modeling technique of fiber pullout from a cement matrix with different interface mechanical properties using finite element program, *Lat. Am. J. Solids Struct.* 2016; 13(10): 1937–1953.

[15] A Babiker, U Häussler-Combe, A Dean, SEM Ahmmed, E Mahdi. Numerical Modeling of Concrete Spallation at Medium Strain-rate, *FES J. Eng. Sci.* 2021; 9(1): 112–120.

[16] S Novikov, I Divnov, A Ivanov. The study of fracture of steel, aluminium and copper under explosive loading, *Fiz. Met. i Metalloved.* 1966; 21(4): 608–615.

[17] LE Schwer, YD Murray. A three-invariant smooth cap model with mixed hardening, *Int. J. Numer. Anal. Methods Geomech.* 1994; 18(10): 657–688.

[18] LE Schwer. Viscoplastic augmentation of the smooth cap model, *Nucl. Eng. Des.* 1994; 150(2–3): 215–223.

[19] LE Schwer, YD Murray. Continuous surface cap model for geomaterial modeling: A new LS-DYNA material type, *7th Int. LSDYNA Users Conf.* 2002; 2: 35–50.

[20] Livermore Software Technology Corp, *LS-Dyna Theory Manual r.* 2019; *11261*: 19.

[21] H Jiang, J Zhao. Calibration of the continuous surface cap model for concrete, *Finite Elem. Anal. Des.* 2015; 97: 1–19.

[22] JC Simo, JW Ju. Strain- and stress-based continuum damage models-I. Formulation, *Int. J. Solids Struct.* 1987.

[23] MB Rubin, Simple, Convenient Isotropic Failure Surface, *J. Eng. Mech.* Feb 1991; 117(2): 348–369.

[24] T-L Teng, Y-A Chu, F-A Chang, B-C Shen, D-S Cheng, Development and validation of numerical model of steel fiber reinforced concrete for high-velocity impact, *Comput. Mater. Sci.* Mar 2008; 42(1): 90–99.